Journal of Sound and Vibration (2001) **245**(3), 483–510
doi:10.1006/jsvi.2001.3594, available online at http://www.idealibrary.com on IDEAL®

RECONSTRUCTION OF ACOUSTIC TRANSFER MATRICES BY INSTATIONARY COMPUTATIONAL FLUID DYNAMICS

W. POLIFKE

Technische Universität München, D-85747 Garching, Germany.
E-mail: polifke@td.mw.tum.de

A. PONCET

ABB Corporate Research Ltd., CH-5405 Baden, Switzerland

AND

C. O. PASCHEREIT AND K. DÖBBELING

Alstom Power Ltd., CH-5405 Baden, Switzerland

(*Received* 15 *June* 2000, *and in final form* 4 *January* 2001)

Thermoacoustic combustion instabilities are a frequently encountered problem in the operation of combustion equipment. The "brute-force" application of computational fluid dynamics to the analysis of thermoacoustic instabilities is estimated to be forbiddingly expensive for many systems of technical interest due to the high computational demands of a time- and space-accurate simulation of a (low Mach number) compressible reacting flow in a complex geometry. Thermoacoustic systems can be modelled efficiently as networks of acoustic multi-ports, where each multi-port corresponds to a certain component of the system, e.g., air or fuel supply, burner, flame, combustor and suitable terminations, and is represented mathematically by its transfer matrix. For some multi-ports, the transfer matrix can be derived analytically from first principles: i.e., the equations of fluid motions and suitable approximations. However, the acoustic behavior of more complicated components, e.g., a burner or a flame, has to be determined by empirical methods, by using a "black box" approach common in communications engineering. In this work, a method is introduced which allows one to reconstruct the transfer matrix of an acoustic two-port from an instationary computation of the response of the two-port to an imposed perturbation of the steady state. Firstly, from the time series data of fluctuating velocity and pressure on both sides of the two-port, the auto- and cross-correlations of the fluctuations are estimated. Then, the unit impulse responses of the multi-port are computed by inverting the Wiener–Hopf equation. Finally, the unit impulse responses are z-transformed to yield the coefficients of the transfer matrix. The method is applied to the one-dimensional model of a heat source with time delay placed in a low-Mach-number compressible flow, for which an analytical description can be derived from first principles. Computational predictions of the transfer matrix have been validated successfully against these analytical results. Furthermore, a comparison of the novel approach presented in this paper with a method for computing the frequency response of a flame by Laplace-transforming its step response is carried out.

1. INTRODUCTION

Thermoacoustic instabilities are a cause for concern in combustion applications as diverse as domestic heating, gas turbines or rocket engines. Combustion instabilities can not only

increase emissions of noise or pollutants such as unburnt hydrocarbons or oxides of nitrogen, but also lead to very high levels of pressure pulsations, resulting in structural damage of the confinement of the flame. For example, in solid propellant rocket motors, pulsation levels as large as 10% of the mean operating pressure have been observed [1]. For stationary gas turbines, the drive for lower emissions of oxides of nitrogen has led to the widespread introduction of premix burners and convectively cooled combustion chambers during the last decade, resulting in reduced flame stability or flame "anchoring" and lower acoustic damping respectively. Consequently, the awareness of thermoacoustic combustion phenomena in gas turbine combustors has increased sharply.

Thermoacoustic instabilities involve a feedback cycle comprising fluctuations in velocity, pressure and heat release rate and possibly also equivalence ratio, entropy or vorticity. Lord Rayleigh [2] deduced a fundamental stability criterion for thermoacoustic oscillations: instationary heat release can enhance acoustic oscillations if the heat release rate peaks at the moment of greatest compression. Note that this criterion provides merely a necessary, but not a sufficient condition for instability, as it does not take into account the stabilizing influence of dissipation of acoustic energy or losses at system boundaries. Nevertheless, Rayleigh's criterion expresses essential physical insight into the problem of thermoacoustic stability, and it emphasizes that stability analysis of a combustion system requires detailed knowledge of the phase relationships between pressure oscillations and the various processes controlling the rate of heat release. This is also the case for more advanced methods of stability analysis (see, e.g., references [3, 4]).

The quantitative modelling of thermoacoustic phenomena with computational fluid dynamics (CFD) is a formidable challenge, as one deals usually with non-stationary turbulent reacting flows, where despite the low Mach numbers prevalent in many applications, the changes of local density with local pressure play an essential role. The propagation of acoustic waves in the combustor and the supply ducts of air and fuel as well as the reflection of acoustic waves at the boundaries of the computational domain must be captured with low dissipation and dispersion errors. Dispersion errors are particularly problematic in the present context, as they influence the phase relationship between fluctuations of velocity or pressure and heat release. To complicate matters, thermoacoustic problems often involve disparate length and time scales: e.g., acoustic wavelengths are often much larger than fluid dynamic length scales. Similarly, the ratio between the frequency and the growth rate of an acoustic disturbance can be very large and indeed tends to infinity as neutral stability (with zero growth rate) is approached. This implies that in an unsteady CFD calculation of a marginally stable situation, a very large number of cycles has to be simulated with high temporal accuracy, resulting in excessive computing time.

Upon considering these obstacles against the direct, "brute force" application of CFD tools to the study of thermoacoustic combustion instabilities, the successes in this area reported by several authors, see, e.g., references [5–11] are remarkable. Although usually restricted to two-dimensional domains with plane acoustic waves, or to very simple three-dimensional cases, these studies have often reproduced experimentally observed behavior and contributed to the understanding of the interaction between fluctuations of velocity, pressure and the location and rate of heat release. Nevertheless, for geometries of applied interest, e.g., an annular gas turbine combustor with several burners, an unsteady simulation of combustion instabilities is still a vision of the future. Instead, acoustic multi-port or network models (see reference [12]) are widely used. In this framework, a combustion system is modelled as an ensemble (a "network") of acoustic multi-ports, with each multi-port representing some component of the system, e.g., fuel or air supply, burner, combustion chamber, cooling channels, etc. (see Figure 1).

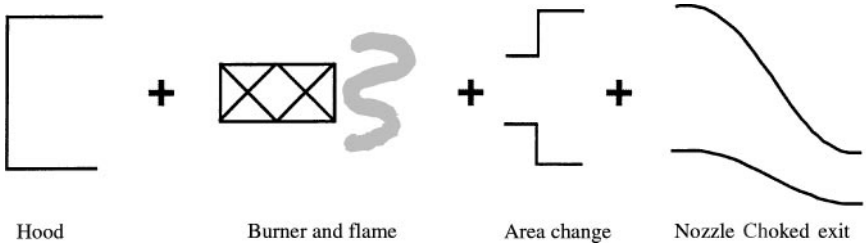

Figure 1. Conceptual model of a combustor as a network of acoustic elements.

Although originally developed for one-dimensional acoustics, i.e., plane wave propagation, the extension to higher order modes in cylindrical or annular geometries is straightforward [13–16].

Under the assumption of linear acoustics and harmonic time dependence $\sim\exp(\mathrm{i}\omega t)$, with network models the system dynamics is represented in frequency space. The unknowns of the system are the complex-valued amplitudes of acoustic variables at the terminations of the elements. The equations of linear acoustics or empirical input are then used to provide coupling relations for the acoustic variables—i.e., the Fourier transforms of fluctuations of pressure p' and velocity v'—across every element. With two variables on the "upstream" and "downstream" sides of a two-port (with indices u and d, respectively), the general form of the coupling is expressed via a so-called *transfer matrix* $\mathbf{T}$:

$$\begin{pmatrix} \hat{p}_d \\ \hat{Z}_d \\ \hat{v}_d \end{pmatrix} = \mathbf{T} \begin{pmatrix} \hat{p}_u \\ \hat{Z}_u \\ \hat{v}_u \end{pmatrix} = \begin{pmatrix} T^{(pp)} & T^{(vp)} \\ T^{(pv)} & T^{(vv)} \end{pmatrix} \begin{pmatrix} \hat{p}_u \\ \hat{Z}_u \\ \hat{v}_u \end{pmatrix}. \tag{1}$$

Here, the characteristic impedance Z—the product of density ρ and speed of sound c—has been introduced to assure dimensional consistency. Alternatively, a thermoacoustic network can be formulated in terms of the Riemann invariants p^+ and p^-, and instead of the transfer matrix, the scattering matrix, which is a 2×2 matrix related to the transfer matrix $\mathbf{T}$ by a linear transformation, can be used [17–19]. Also, if fluctuations of, say, equivalence ratio or entropy are involved, such that a total of n input and m output variables are linked via the multi-port, the transfer matrix will be of dimension $m\times n$ [16, 20, 21].

The description of the thermoacoustic characteristics of a complete combustion system as a linear system of equations $\mathbf{S}\cdot\mathbf{u}=\mathbf{d}$ is obtained by combining the coefficients of the transfer matrices of all elements into one system matrix $\mathbf{S}$ and all unknowns in one vector $\mathbf{u}$. Once the system matrix is generated, both the stability with respect to self-excited oscillations [3] as well as the response to an external or fluid-mechanic internal excitation can be analyzed. In the latter case, the vector $\mathbf{d}\neq 0$ represents the driving forces in the system.

Obviously, the application of these tools requires knowledge of the transfer matrices of the system's constituent multi-ports. The transfer matrix of simple multi-ports can be derived from the (linearized) equations of conservation of mass and momentum and suitable additional assumptions. This approach is widely used, the works by Deuker [22], Keller [13], Dowling [20] or Polifke *et al.* [16] may serve as recent examples.

However, in general the determination of all relevant transfer matrices from first principles is intractable, and one has to resort to empirical input. For the purpose of measuring transfer matrices in experiments, Paschereit and Polifke [17] have developed an extension of the "black box" approach used in communications engineering. This method

had been employed previously to describe fluid machines in enclosures, e.g., fans or pumps, as acoustical multi-ports (see, e.g., references [23–25]). For further details, the reader is referred to references [17–19].

With a "black box" approach, it is not necessary to formulate an analytical model for the multi-port, i.e., closed-form expressions describing the dependence of the transfer matrix' coefficients on frequency, mean flow properties, geometrical parameters, etc. Instead, coefficient values determined empirically for certain operation conditions and over a range of frequencies may be used via look-up tables or suitable interpolations in network models to investigate the stability against self-excited oscillations or to compute the response to a driving mechanism.

Experience with the experimental determination of transfer matrix coefficients has shown that this approach requires very high experimental precision, sophisticated post-processing of large amounts of raw experimental data and long test runs, if the transfer matrix is to be recorded over a range of frequencies. Application of the method to combustors at elevated pressures is expected to be very difficult and expensive. Therefore, it seems attractive to explore the possibility of obtaining information on the dynamical behavior of a multi-port —a burner or a flame, say—from numerical simulation. Generally speaking, one possible realization of this idea is to carry out a time-dependent simulation of the dynamical behavior of the multi-port and somehow *reconstruct* the desired information—ideally the complete transfer matrix—from the time series data. The overall system behavior is then investigated again with the network method, by making use of a combination of transfer matrices obtained from first principles as well as experiment or simulation.

The advantages of such an approach over the "brute force" modelling of combustion instabilities should be the following: instead of simulating and recording the evolution of a complete thermoacoustic system over many cycles until a steady state or limit cycle is reached, only the dynamics of a single network element has to be tracked until a sufficient amount of information has been collected to reconstruct the transfer matrix. Also, it should be possible to curtail the computational domain to include only the multi-port of interest and its immediate surrounding. This should reduce significantly both the memory and CPU time requirements. Furthermore, with the reduced size of the computational domain, errors in acoustic signal propagation due to numerical dissipation and dispersion do not accumulate over long distances.

The idea of extracting dynamical characteristics of a flame from time-dependent simulation and then using this information in linear acoustic analysis has first been explored by Sklyarov and Furletov [26] for a one-dimensional laminar flame, then by Bohn and Deuker [27] and Deuker [22] for a V-shaped laminar flame and more recently by Krüger *et al.* [28, 29] for a turbulent flame and a gas turbine burner respectively. In these studies, the response of the flame to a sudden increase in mass flow rate—the *unit step response*, or simply the *step response*—is determined in a time-dependent CFD simulation. The step response is then Laplace-transformed into frequency space, yielding the frequency response function. This frequency response function equals—upto normalization factors—one of the coefficients of the transfer matrix, i.e., the coefficient $T^{(vv)}$, which couples velocity fluctuations across the flame. In order to obtain a complete description of the flame's thermoacoustic characteristics, analytical expressions for the remaining three coefficients of the transfer matrix are introduced, based on suitable approximations.

In this paper, an alternative method is proposed, whereby the *impulse response* functions of a multi-port are determined from instationary CFD simulation with randomly perturbed boundary conditions. Subsequently, the impulse responses are z-transformed to obtain the complete transfer matrix. For the purpose of confirming the validity and exploring the accuracy of this novel approach, it is applied in this work to a simple, one-dimensional

thermoacoustic system which has been designed to exhibit sufficiently interesting thermoacoustic characteristics, be simple enough to also make possible "brute force" modelling of thermoacoustic instabilities at low computational cost, and allow for analytical modelling in order to compare numerical results against known solutions.

The paper is organized as follows: in the next section, the one-dimensional thermoacoustic system is introduced, which serves as a test bed for the novel method. Linearizing the functional dependence of heat release rate and pressure drop on flow velocity at the heat source yields the transfer matrix of the heat source. By using a network model, the stability characteristics of the test system are then determined to be used later for validation purposes. In section 3, growth rates obtained from a "brute force" time-dependent simulation are compared against analytically determined growth rates. Then, the approach developed by Sklyarov and Furletov [26] and Deuker [22] for determining the flame transfer function by Laplace-transforming the step response is applied to the test system, the results and experiences are discussed critically. In the subsequent section, the novel approach, based on the z-transform of the impulse responses, is presented. The modifications required to apply the method also to multi-ports with more than one input and output are described in detail. In section 6, the impulse responses and the transfer matrix extracted from a time-dependent computation of perturbed flow across the heat source in the one-dimensional model are presented and compared against analytical findings.

2. THE τ–ζ MODEL

Consider compressible flow in a straight duct of length L with a heat source placed in its middle. By analogy with the Rijke tube [30] or the n–τ model [31], thermoacoustic instabilities may occur if the momentary heat-release rate per unit area $\dot{Q}(t)$ depends on the velocity v of the flow across the region of heat release at an earlier time,

$$\dot{Q}(t) = \dot{Q}(v_c(t-\tau), \dots), \tag{2}$$

where τ is the *time lag* of the system (a list of nomenclature is given in Appendix C). To take the analogy with heat transfer at the gauze of a Rijke tube a bit further, it is assumed in the following that the momentary heat release rate follows King's Law [30], which describes conduction and laminar convection of heat from a hot wire in a cross-flow,

$$\dot{Q}(t) = L_W(T_W - T)[\kappa + 2\sqrt{\pi\kappa\rho c_v r|v_c(t-\tau)|}], \tag{3}$$

where L_W is the total length of wire per unit cross-sectional area of the duct, T the temperature of the wire, r its radius, and κ, ρ, c_v the thermal conductivity, the density and specific heat at constant volume of the gas respectively. For laminar flow across the wire, the time lag τ is determined by the inertia with which the boundary layer of the wire can adjust to changes in the free stream velocity. However, for the present purpose, τ is simply regarded as a freely adjustable parameter, which controls—among other factors—stability of the system. If the flow velocity is sufficiently large, pure conduction of heat is negligible, and with $A = 2L_W(T_W - T)\sqrt{\pi\kappa\rho c_v r}$, equation (3) can simply be written as

$$\dot{Q}(t) = A\sqrt{|v_c(t-\tau)|}. \tag{4}$$

To make the heat release model a bit more interesting, a second freely adjustable parameter is introduced, i.e., a pressure loss coefficient ζ, which controls the pressure drop

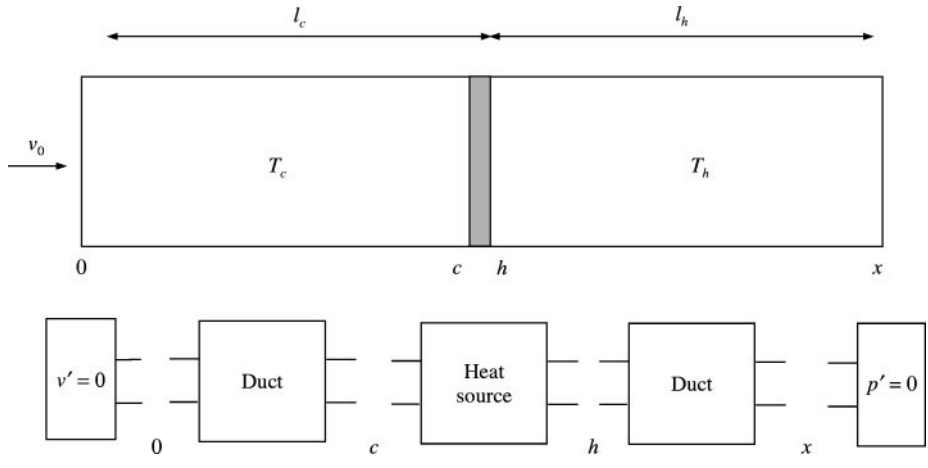

Figure 2. Sketch of the model system investigated in the study (top) and its network representation (bottom). Mean flow is from left to right.

Δp across the heat source,

$$\Delta p \equiv p_c - p_h = \tfrac{1}{2}\rho\zeta v_c^2. \tag{5}$$

The subscripts c and h stand for the cold (upstream) and hot (downstream) side of the heat source. One may expect that with increasing pressure loss coefficient ζ, the stability with respect to self-excited thermoacoustic oscillations will increase, as well. To facilitate the implementation of this configuration in a standard CFD code, the boundary conditions are prescribed as follows: constant velocity $v(x = 0) = v_0$ at the inlet and constant static pressure $p(x = L) = const.$ at the outlet of the duct. The first acoustic eigenmode of the system with these boundary conditions is the well-known quarter-wave mode. With the region of heat release positioned in the middle of the duct, the phase relationship between the fluctuations of velocity and pressure at the heat source is identical to the one found in a standard Rijke tube with two open ends and the heat source placed at $x = L/4$.

In analogy with the Rijke-tube and the n–τ model [3, 30, 31], alternating bands of stability and instability for the fundamental mode and higher order acoustic modes should be expected when the time lag τ is increased. This can be confirmed by setting up the network representation of the system and determining its eigenfrequencies for varying values of τ. A sketch of the model system and its network representation is shown in Figure 2. The boundary condition $v(x = 0) = v_0$ at the cold side of the duct implies that

$$v_0' = 0$$

and similarly

$$p_x' = 0,$$

due to the pressure boundary condition prescribed at the outlet. The transfer matrix describing the propagation of an acoustic signal in a duct is well known,

$$\begin{pmatrix} \dfrac{\hat{p}_j}{\rho_j c_j} \\ \hat{v}_j \end{pmatrix} = \begin{pmatrix} \cos\ \alpha & \mathrm{i}\sin\alpha \\ \mathrm{i}\sin\alpha & \cos\alpha \end{pmatrix} \begin{pmatrix} \dfrac{\hat{p}_i}{\rho_i c_i} \\ \hat{v}_i \end{pmatrix}, \tag{6}$$

with $\alpha = kL/(1 - M^2)$ and wave number $k = \omega/c$. For the cold side of the test system, the indices $\{i, j\} = \{0, c\}$, while for the hot side $\{i, j\} = \{h, x\}$.

The transfer matrix of the heat source, coupling nodes "c" and "h", is obtained by linearization of the Rankine–Hugoniot relations, which express conservation of mass, momentum and energy across a thin heat source [32]. This derivation is also given in reference [16] and shall not be repeated here. The resulting relation between the fluctuations of velocity on both sides of a heat source is

$$v'_h(t) = v'_c(t) + \left(\frac{T_h}{T_c} - 1\right) v_c \left(\frac{\dot{Q}'(t)}{\dot{Q}} - \frac{p'_c(t)}{p_c}\right). \tag{7}$$

Linearizing equation (3) for small fluctuations v'_c around a positive mean velocity v_c yields

$$\frac{\dot{Q}'(t)}{\dot{Q}} = \frac{v'_c(t - \tau)}{v_c}. \tag{8}$$

With $c^2 = \gamma p/\rho$ and the definition

$$n \equiv \frac{1}{2}\left(\frac{T_h}{T_c} - 1\right),$$

equation (7) can be rewritten as

$$v'_h(t) = v'_c(t) + n v'_c(t - \tau) - 2n\gamma M_c \frac{p'_c(t)}{Z_c}, \tag{9}$$

or equivalently in the frequency domain

$$\hat{v}_h = \hat{v}_c(1 + n\,\mathrm{e}^{-\mathrm{i}\omega\tau}) - 2n\gamma M_c \frac{\hat{p}_c}{Z_c}. \tag{10}$$

The first term on the r.h.s. is the familiar transfer function of the n–τ model [31], with an *interaction index* n and time lag τ. Note that in the present context, n is not a freely adjustable parameter, but depends on the values of the mean temperatures on both sides of the heat source. The factor $\frac{1}{2}$ appears in the definition of the interaction index n because it is assumed that the fluctuations in heat release rate are proportional to the square root of the velocity, see equation (3).

For the pressure, the linearized Rankine–Hugoniot relations are

$$p'_h(t) = p'_c(t) - \left(\frac{T_h}{T_c} - 1\right)\rho_c v_c^2 \left(\frac{v'_c(t)}{v_c} + \frac{\dot{Q}'(t)}{\dot{Q}}\right) - \zeta \rho_c v_c v'_c(t). \tag{11}$$

Up to the additional pressure loss term, this is equation (13) in reference [16]. With the definitions introduced above and the linearized form of relation (3) between heat release rate and velocity, one obtains

$$\frac{\hat{p}_h}{Z_h} = \frac{\hat{p}_c}{Z_c} - \xi M_c(2n + n\,\mathrm{e}^{-\mathrm{i}\omega\tau} + \zeta)\,\hat{v}_c. \tag{12}$$

Combining the two linearized Rankine–Hugoniot relations for velocity and pressure fluctuations, one obtains the transfer matrix of the heat source:

$$\begin{pmatrix} \hat{p}_h \\ \overline{Z_h} \\ \hat{v}_h \end{pmatrix} = \begin{pmatrix} \xi & -\xi M_c(2n + n\,\mathrm{e}^{-\mathrm{i}\omega\tau} + \zeta) \\ -2n\gamma M_c & 1 + n\,\mathrm{e}^{-\mathrm{i}\omega\tau} \end{pmatrix} \begin{pmatrix} \hat{p}_c \\ \overline{Z_c} \\ \hat{v}_c \end{pmatrix}. \tag{13}$$

The time lag τ and the pressure loss coefficient ζ are two freely adjustable parameters which control the dynamic characteristics of the heat source and the stability of the system. In analogy with the well-known n–τ model, the model just introduced shall be referred to as the τ–ζ model in the following.

Comparing the transfer matrix of the τ–ζ model with the one given by Heckl [30] for the gauze in a Rijke tube, one notices that Heckl has omitted the off-diagonal terms. This certainly is a permissible approximation, as the flow in a Rijke tube is induced by free convection and the Mach number is very small indeed. The off-diagonal terms are also often neglected in models for the thermoacoustic behavior of flames [22, 28, 29] again with the justification that in technical applications, Mach numbers larger than $M_c = 0{\cdot}1$ are rarely encountered. However, it has been shown [16, 18] that for a compact premixed flame, the off-diagonal coefficients of the transfer matrix are of order $(T_h/T_c - 1)M_c$: i.e., the Mach-number scaling is the same as in equation (13). With temperature ratios larger than 5 in stoichiometric flames, $\mathbf{T}^{(vp)}$ and $\mathbf{T}^{(pv)}$ are not much smaller than unity even at moderate Mach numbers M_c of order 10^{-1}. This is especially so if instead of a flame sheet, the transfer matrix of a complete burner[†] is considered. For modern premix burners, which spend a significant portion of the available dynamic head for mixing of fuel and air, the "acoustic" pressure loss coefficient ζ is of order 10, say, and the upper right coefficient $\mathbf{T}^{(vp)}$ of the transfer matrix may be quite large [17]. Indeed, a recent study [33] indicates that under certain circumstances, this coefficient may be the primary cause of unstable combustion.

To summarize, the τ–ζ model as it has been formulated in equations (3), (5) and (13), describes in the limit of low Mach numbers (and with zero pressure loss coefficient ζ) the heat transfer at the gauze of a Rijke tube in laminar flow. On the other hand, with larger values of Mach number M_c and non-zero loss coefficient ζ, this simple heat release model shares many characteristics with realistic premix burners, as far as the thermoacoustic properties are concerned.

Once all required transfer matrices have been determined, it is straightforward to set up the system matrix $\mathbf{S}$ for the test system (see Figure 2). Details have been presented by Gijrath [34] and Löfgren [35]. All transfer matrices are known analytically, i.e., in closed form in terms of mean flow and model parameters, geometry and frequency ω. The simplest way to carry out a stability analysis is, in this case, to search numerically for the eigenfrequencies ω, which satisfy the characteristic equation $\mathrm{Det}(\mathbf{S}) = 0$. Real and imaginary parts of the fundamental quarter-wave mode's eigenfrequencies ω_1 obtained from such calculations for varying values of time lag τ are shown in Figure 3. With the sign conventions used in this paper, negative values of the imaginary part indicate instability, so as expected, alternatively stable and unstable system behavior is found, depending on the value of τ. This pattern is repeated with yet higher values of the time lag τ and also for the higher modes (not shown). In the next section, the τ–ζ model system will be simulated with a CFD code and predictions of frequencies and growth rates obtained with the fluid dynamic simulation are compared against analytical results.

[†] Fuel injector nozzle, premixing section and flame are designated as *burner* in this paper.

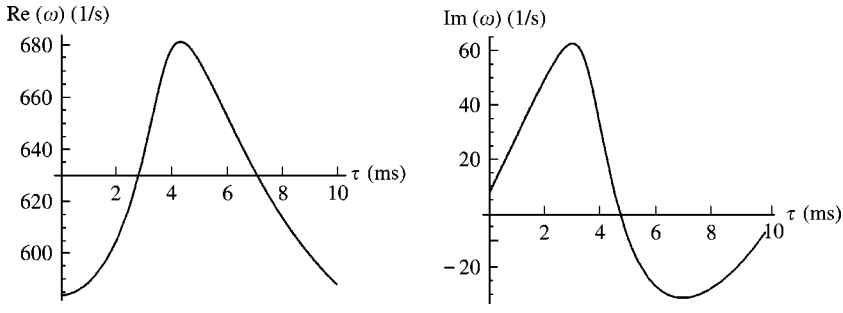

Figure 3. Stability analysis of the τ–ζ model: Real part (left) and imaginary part (right) of the eigenfrequency ω of the fundamental mode for varying values of the time lag τ and interaction index $n = 0{\cdot}25$. For this computation, $l_c = l_h = 0{\cdot}5$ m, $T_c = 288$ K, $T_h = 433$ K, $v_0 = 10$ m/s, $\gamma = 1{\cdot}4$.

3. CFD SIMULATION OF THE τ–ζ MODEL

Many of the studies of thermoacoustic combustion instabilities with computational fluid dynamics (CFD) tools found in the literature use standard algorithms, usually of the pressure correction type [6, 7, 9, 10]. This should come as a surprise—after all, low-Mach-number compressible flows are notoriously difficult to compute efficiently and accurately and the use of appropriate numerical methods is recommended [36]. Nevertheless, when confronted with the task of developing a special purpose code for thermoacoustic calculations in geometries of applied interest, including necessarily not only an appropriate formulation of the fluid dynamics and advanced numerics, but also models for turbulence and combustion plus the ability to handle large, complex geometries, it appears that many researchers have decided to use standard, validated numerical tools, based on a SIMPLE type algorithm, second order spatial discretization and first or second order temporal accuracy. Indeed, the authors' experience with simple, one-dimensional acoustic test cases for which analytical solutions are known, confirms that such codes can produce acceptable results, provided that the time steps are small enough—at least 100 time steps per cycle were required for the test cases investigated by Gijrath [34] and Löfgren [35]. For this reason, for the numerical studies reported here, a standard, finite volume based CFD code with a SIMPLE pressure correction scheme was used.

It is fairly straightforward to implement the τ–ζ model for heat release and pressure loss in a CFD code via appropriate source terms for enthalpy and momentum, according to equations (3) and (5) respectively. Note that the relations (7), (11) and (13), which were derived by linearizing the conservation equations for mass, momentum and energy in terms of small fluctuations p', v' and $\dot{Q}'$, do not appear explicitly in the numerical formulation. In this sense, the CFD model is not an acoustic, but a fluid dynamic model. In order to obtain the required time lag between fluctuations of velocity v_c' and heat release $\dot{Q}$, the velocity history just upstream of the heat source is stored in computer memory and retrieved after the appropriate time to set the momentary heat release rate according to King's Law (3) during a time-dependent simulation.

The geometry of the test system is one-dimensional with 200 cells in the x direction. Note that the heat source is distributed over five computational cells, with the rate of heat release highest in the center of this group of cells. This slight "smearing out" of the heat release was required to avoid divergence problems with higher order spatial discretization. Although the heat release is distributed over five cells, the heat source can certainly be considered to be compact, as the length of the region of heat release is less than one-thousandth of the wavelength of the fundamental mode, i.e., the quarter wave mode of the tube.

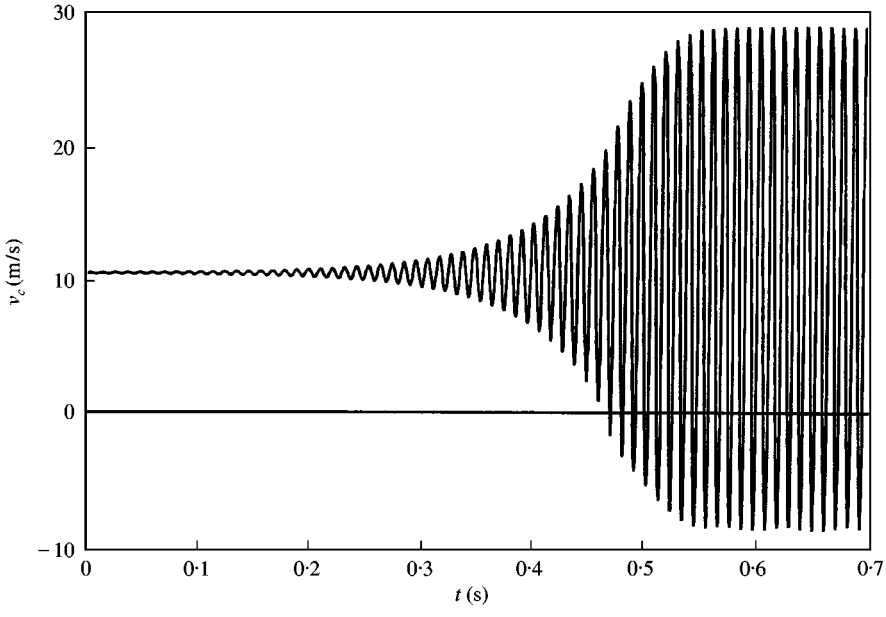

Figure 4. Velocity v_c just upstream of the heat source in the τ–ζ tube during build-up of a limit cycle. Time lag $\tau = 7$ ms corresponding to the most unstable case according to linear stability analysis.

To initialize the flow and temperature distributions in the tube for the unsteady simulation, first a stationary solution was computed. To obtain such a "base flow" will be difficult, if the base flow corresponds to a thermoacoustically unstable configuration. Then, the self-excited combustion instability will manifest itself as divergence difficulties for the stationary solver. To avoid such divergence problems, an incompressible fluid model was used for the base flow; i.e., the density ρ would not depend on local changes of the static pressure. In this way, the thermoacoustic feedback loop was broken, and the base flow could be computed without difficulties. The base flow velocity distribution was then perturbed randomly by 5% of its respective mean value, compressibility was "switched on", and the time-dependent simulation started.

A typical result is shown in Figure 4. Here, the operating conditions are those analyzed in the previous section with linear acoustics, i.e., the network model. The time lag chosen is $\tau = 7$ ms, corresponding to maximum growth rate. Indeed, it was observed that after a gestation period of approximately 0·1 s duration, during which the random initial perturbations evolve into a coherent, $\frac{1}{4}$-mode standing wave, the amplitudes grow rapidly, Saturation of the growth occurs not before the velocity at the heat source is negative (!) during part of the cycle. The reverse flow transports hot fluid back over the heat source, thereby reducing the temperature difference $T_W - T$, which drives the transfer of heat to the fluid. This reduction in heat flux and non-linear transfer of acoustic energy to higher modes [7] eventually leads to saturation of the instability, and a limit cycle is established. Note that all amplitudes of pressure fluctuations in the limit cycle are less than 1% of the operating pressure, so, it is only the heat source which behaves essentially non-linearly, while the acoustics may still be treated in the linear approximation.

If a time lag $\tau = 3$ ms is chosen, the initial disturbances decay very rapidly, i.e., within less than 10 cycles. A quantitative comparison of growth rates, or rather *cycle increments*

$$\delta = \exp\left\{-2\pi \frac{\mathrm{Im}(\omega)}{\mathrm{Re}(\omega)}\right\} - 1, \tag{14}$$

TABLE 1

Comparison of frequencies and cycle increments predicted with linear stability analysis and unsteady CFD computation; for the stable case , the time lag $\tau = 3$ ms, *while for the unstable case,* $\tau = 7$ ms

	Stability analysis	Unsteady CFD
Stable case		
Frequency Re(ω) (s^{-1})	641	465
Cycle increment	−0·46	−0·50
Unstable case		
Frequency Re(ω) (s^{-1})	635	591
Cycle increment	0·35	0·16

and frequencies Re(ω) obtained with CFD and network stability analysis is given in Table 1. The cycle increment is defined in this work as the fraction by which a pulsation amplitude increases during one cycle. Neutral stability corresponds to $\delta = 0$. The predicted cycle increment $\delta = 0{\cdot}35$ for the unstable case $\tau = 7$ ms is very large. Such an unrealistically large cycle increment is possible only because all mechanisms which result in loss of acoustic energy like radiation of sound at the open end or viscous dissipation in the wall boundary layer have been neglected in the idealized τ–ζ model. From the CFD runs, frequency and growth rate were obtained by non-linear, least-squares fitting of an exponential function to the time series data in the time interval $0{\cdot}1 \text{ ms} < t < 0{\cdot}45$ ms: i.e., up to the moment where reverse flow and reduced growth sets in. The cycle increment δ obtained by CFD is lower than it should be, indicating that dissipative losses and dispersive errors are not negligible. Note that because $\tau = 7$ ms corresponds to maximum growth rate, i.e., most favorable phase between fluctuations of heat release and pressure, phase errors will always decrease the growth rate for this case.

The same fitting procedure was applied to data from the stable case, where the initial perturbations decay quickly. However, only very few cycles can be observed before the perturbations die out, therefore the agreement between the predictions of CFD and linear stability analysis is not very convincing, especially for the frequency.

The CFD model reproduces qualitatively the behavior predicted by linear stability analysis based on the network approach. Furthermore, for the unstable case, a plausible mechanism of saturation by non-linear effects at the heat source can be observed. However, the computed growth rates are not in satisfactory agreement with the results of linear stability analysis. Given the accuracy which can be achieved with the present CFD modelling approach, it seems unlikely that the stability borders, i.e., those values of the time lag τ for which the cycle increment $\delta = 0$, could be predicted correctly. Similar results for cases with higher Mach number and non-zero pressure loss coefficient ζ have been obtained by Löfgren [35].

The reasons for the discrepancies observed are expected to be dissipative losses and phase errors accumulated during the propagation of acoustic waves along the duct. Nevertheless, the simple one-dimensional CFD model of the thermoacoustic system captures correctly the important aspects of system behavior. In particular, the time-delayed, dissipative heat source—see equations (3) and (5)—which has been implemented via appropriate source terms for enthalpy and momentum in a few computational cells, behaves as expected. It therefore makes sense to apply the methods for reconstructing frequency response functions

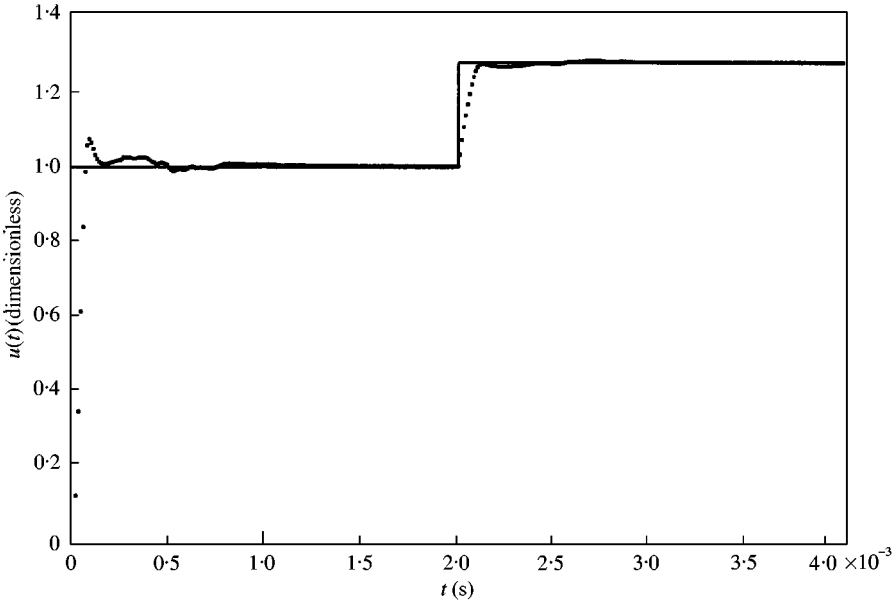

Figure 5. Ideal (——) and computed (·····) unit step response $u(t)$, i.e. the normalized downstream velocity $v'_d(t)$ of the n–τ model for $n = 0{\cdot}28$ and $\tau = 2$ ms.

or transfer matrices from a time-dependent calculation to this CFD model and validate those methods against the analytical result (13).

4. UNIT STEP RESPONSE AND LAPLACE TRANSFORM

Sklyarov and Furletov [26] have determined the velocity–velocity frequency response function $T^{(vv)}$ of a one-dimensional laminar premix flame by computing the Laplace transform of its unit step response. Later, the approach has been extended to turbulent flames and gas turbine burners [22, 27–29]. The mathematical background of the method is briefly summarized in Appendix A.

It is in general not possible to determine a complete transfer matrix (see equation (13)) with this approach. Fortunately, for sufficiently small Mach number M_c and pressure loss coefficient ζ, the off-diagonal terms of the transfer matrix of the $\tau - \zeta$ model are negligible. The pressure–pressure term $T^{(pp)} = \xi$ is equal to the ratio of specific impedances, so the only non-trivial term of the transfer matrix is in this limit the velocity–velocity term $T^{(vv)}$, which is equal to the frequency response function of the n–τ model:

$$T^{(vv)} = 1 + n\,\mathrm{e}^{-\mathrm{i}\omega\tau}. \tag{15}$$

When adopting the Laplace transform formalism to time series data from numerical simulation, one must be aware that a mathematically well-defined discrete version of the forward Laplace transform is not known. Unbehauen [38] has proposed a numerical procedure to determine an approximate Laplace transform, which has been used by Deuker [22] and Krüger *et al.* [28, 29]. Comments on the shortcomings of this procedure are given below.

The unit step response of the τ–ζ model has been computed by Gijrath [34], using the CFD model discussed in the previous section. Results are shown in Figures 5 and 6. The

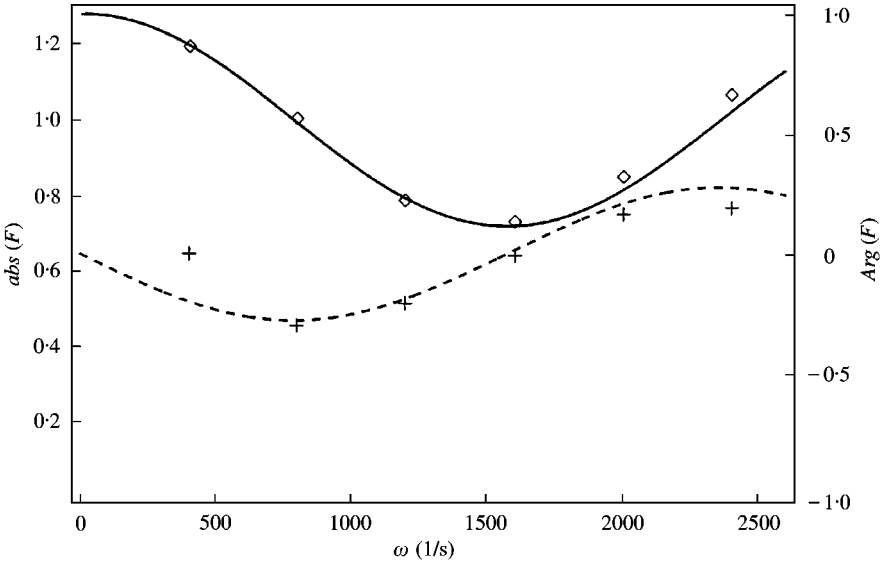

Figure 6. Frequency response function of the n–τ model determined with the Laplace transform of the step response. Absolute value (◇, —, left axis) and argument (+ , - - -, right axis).

parameters for this particular run are the following: upstream velocity $v_c(t < 0) = 20$ m/s, upstream temperature $T_c = 288$ K, downstream temperature $T_h = 440$ K, interaction index $n = 0{\cdot}28$ and time delay $\tau = 2$ ms. The simulation was continued up to a time $t_{max} = 2\tau$.

Figure 5 shows that the CFD model of the heat source indeed reproduces the expected behavior. Deviations from the analytical solution are small and do not last longer than approximately 0·1 ms, so any errors due to these numerical errors should show up only at very high frequencies of several kHz[‡]. Applying the approximate Laplace transform to the time series data then gives excellent agreement for the frequency response function $F(\omega)$; see Figure 6. Up to frequencies $\omega = 2500\ \mathrm{s}^{-1}$, the computed absolute value of the response function matches the analytical value almost exactly. Phase errors are also small, with the exception of the first data point near $400\ \mathrm{s}^{-1}$. The errors grow larger for angular frequencies $\omega > 2500\ \mathrm{s}^{-1}$ [34]; however, this frequency range is irrelevant for stability analysis of the fundamental mode.

To achieve such good agreement, it was necessary to move the location of the heat source to the left end of the computational domain; i.e., the inlet boundary "0". If the heat source is located further downstream from the inlet, then the perturbation signal smears out very strongly due to numerical dissipation, and the heat source no longer encounters a Heaviside signal (not shown).

Besides the suppression of numerical diffusion, another reason for moving the heat source for the response computation towards the inlet are spurious distortions of the response signal due to reflections. The original perturbation, after passing the heat source, is reflected at the outlet boundary condition—unless a non-reflection boundary condition is implemented, which is usually not the case in pressure-correction codes—and eventually

[‡] Indeed, the Rankine–Hugoniot relations are valid only if quasi-steady conditions prevail at the heat source, i.e., the rate of change of the upstream conditions should be larger than the time $t \approx 0{\cdot}5$ ms which is required for the mean flow to flow past the heat source. This is not the case for a Heaviside signal, so deviations from the Rankine–Hugoniot relations are expected to occur for very high frequencies even if numerical diffusion could be suppressed completely by an appropriate numerical scheme.

perturbs the heat source a second time. If this happens, an incorrect step response will be recorded, leading to erroneous prediction of the frequency response. When moving the heat source to the left of the domain, it is possible to record the response up to a time $t_{max} = 2\tau$ for the chosen value of the time lag $\tau = 2$ ms.

Unbehauen [22, 38] has shown that the following relation must be satisfied for the frequencies ω at which the numerical Laplace transform can be evaluated:

$$\omega = \frac{\pi(m + \frac{1}{2})}{t_{max}}, \tag{16}$$

where $m = 0, 1, 2, \ldots$. Therefore, the sampling time t_{max} limits the minimum frequency and the frequency spacing $\Delta\omega$ which can be achieved with the numerical forward Laplace transform. In the present case, $\Delta\omega = \pi/2t_{max} \approx 400\ \mathrm{s}^{-1}$. Such a large frequency spacing is not sufficient to carry out a stability analysis [3, 4].

In summary, the Laplace transform of time series data taken from an unsteady CFD computation of the step response has reproduced the analytically derived frequency response function with excellent accuracy. However, the following difficulties with this method have become apparent: the method can only be used to determine a scalar frequency response function, and consequently, the method is inadequate if more than one coefficient of the transfer matrix are neither negligibly small nor known from first principles; the steep gradients of the unit step perturbation are difficult to resolve accurately due to numerical dispersion or—if higher order discretization schemes are employed—due to overshoots and convergence difficulties; short sampling times t_{max} lead to unacceptably large minimum frequencies and frequency spacings, but on the other hand, with increasing t_{max}, one very soon faces the problem that reflections from the downstream boundary distort the response to the unit step signal.

In the next section, a novel method based on the unit impulse response and the z-transform is presented, which does not suffer from any of these deficiencies.

5. SYSTEM IDENTIFICATION WITH THE UNIT IMPULSE RESPONSE

The method for determining the frequency response function by computing the Laplace transform of the unit step response is a basic example of *system identification*. Advanced techniques for system identification have been developed in communications engineering. In this section, the transfer matrix of an acoustic element is determined from a time-dependent numerical simulation via the *impulse responses* of the element. Background material on system identification and in particular the mathematical techniques presented below can be found in references [39–41].

Consider the values of acoustic variables upstream of the element as a signal s and the downstream values as the corresponding response r. Data taken with a certain sampling rate from experiment or from a time-dependent numerical simulation will provide time series

$$s_i = s(\mathrm{i}\Delta t), \quad i = 0, \ldots, N,$$

and similarly for the response r_i. Here Δt is the sampling rate, which may be equal to or a multiple of the time step of the numerical simulation. The action of the element on the incoming signal, i.e., the coupling between response r and signal s can be approximated as

$$r_i \approx \tilde{r}_i = \sum_{k=0}^{L} h_k s_{i-k} \quad \text{for } i = L, \ldots, N. \tag{17}$$

In the terminology of digital signal processing [40], equation (17) describes a *finite impulse response* (FIR) filter. If the signal is just a single peak of unit amplitude at time $t = 0$, $s_i = \delta_{i0}$, where the Kronecker δ_{ij} equals unity if $i = j$ and otherwise zero, then with equation (17)

$$\tilde{r}_i = \sum_{k=0}^{L} h_k \delta_{ik} = h_i.$$

Obviously, the vector $\mathbf{h} = \{h_k;\ k = 0, \ldots, L\}$ is the filter's response to the unit impulse δ_{i0} and is accordingly named the *unit impulse response* or simply *impulse response* of the filter[§]. If the response of the filter is determined only by the *momentary* value of the excitation signal, then $r_i = a s_i$ and $h_k = a\,\delta_{k0}$, with a being a constant factor; i.e., the filter is memoryless. For general signal series and a linear filter, the response r_i at time $t_i = \mathrm{i}\,\Delta t$ is approximated as a weighted sum over the recent history of the input signal s_{i-k}; $k = 0, \ldots, L$. The coefficients h_k are weighting factors in this summation, and obviously L should be sufficiently large, such that h_k is of negligible magnitude for $k > L$. In other words, the time interval $L\,\Delta t$ must be longer than the filter's "memory" of previous signal states.

To summarize: given a filter with known impulse response $\mathbf{h}$ and a time series $\mathbf{s} = \{s_i;\ i = 0, \ldots, N\}$ of signals, it is straightforward to calculate the response $\mathbf{r} = \{r_i; i = 0, \ldots, N\}$ of the filter. However, in system identification one faces usually the inverse problem: given time series $\mathbf{s}$ and $\mathbf{r}$, how can one estimate the impulse response $\mathbf{h}$ of the filter? The solution to this question provides the Wiener–Hopf equation (also known as the *Wiener equation* or *normal equation*),

$$\Gamma \mathbf{h} = \mathbf{c}, \tag{18}$$

where

$$c_i = \frac{1}{M} \sum_{l=L}^{N} s_{l-i} r_l \quad \text{for } i = 0, \ldots, L, \tag{19}$$

$$\Gamma_{ij} = \frac{1}{M} \sum_{l=L}^{N} s_{l-i} s_{l-j} \quad \text{for } i, j = 0, \ldots, L. \tag{20}$$

Here, $M = N - L + 1$, Γ approximates the *autocorrelation matrix* of the signal $\mathbf{s}$, and $\mathbf{c}$ the cross-correlation vector between $\mathbf{s}$ and $\mathbf{r}$. By inserting the definitions of Γ and $\mathbf{c}$ and substituting for $\mathbf{r}$ with equation (17) one can readily verify equation (18):

$$(\Gamma \mathbf{h})_i = \frac{1}{M} \sum_{j=0}^{L} \sum_{l=L}^{N} s_{l-i} s_{l-j} h_j = \frac{1}{M} \sum_{l=L}^{N} s_{l-i} \sum_{j=0}^{L} h_j s_{l-j} = \frac{1}{M} \sum_{l=L}^{N} s_{l-i} r_i = c_i.$$

With equations (19) and (20), it is easy to compute estimates for the autocorrelation Γ and the cross-correlation $\mathbf{c}$ from time series data and then obtain the impulse response $\mathbf{h}$ by inverting the Wiener–Hopf equation

$$\mathbf{h} = \Gamma^{-1} \mathbf{c}$$

[§] Recalling that the Green function of a differential operator represents the solution or the response to a (Dirac-) δ-source, one may think of the unit impulse response as a discrete, one-sided (causality!) equivalent to the Green function.

with standard methods of (numerical) linear algebra. However, the impulse response "lives" in the time domain. To make use of it in the network analysis of thermoacoustic systems, which is usually fomulated in the frequency domain, it is necessary to transform the impulse response into a transfer function $F(\omega)$. This is accomplished with the z-transform (the equivalent of the Laplace transform for discrete-time systems):

$$\mathbf{h} \to \check{h}(z) \equiv \sum_{k=0}^{L} h_k z^{-k}, \tag{21}$$

with the argument set to $z = \exp\{\mathrm{i}\omega \Delta t\}$, i.e.,

$$F(\omega) = \check{h}(\mathrm{e}^{\mathrm{i}\omega \Delta t}) = \sum_{k=0}^{L} h_k \mathrm{e}^{-\mathrm{i}\omega \Delta t k}.$$

In Appendix B, it is shown in a general form that this transformation indeed produces the desired transfer function between the signal's and the response's Fourier transforms, respectively. Here, the method is applied to the n–τ model of the velocity–velocity coupling. Assume that $\tau = m\Delta t$, with m some integer less than L. Then for the n–τ model

$$h_k = \delta_{k0} + n\delta_{k,m}.$$

This result should be obvious from the definition of $\mathbf{h}$ as the response to a unit impulse signal. The z-transform of the impulse response with argument $\exp\{\mathrm{i}\omega \Delta t\}$ evaluates to

$$\check{h}(\mathrm{e}^{\mathrm{i}\omega \Delta t}) = \mathrm{e}^{-\mathrm{i}\omega \Delta t 0} + n\mathrm{e}^{-\mathrm{i}\omega \Delta t m} = 1 + n\mathrm{e}^{-\mathrm{i}\omega\tau},$$

which is indeed the velocity–velocity transfer function $T^{(vv)}(\omega)$ of the n–τ model.

Although it has not been stated explicitly, the discussion has been limited so far to a one-port with a single input and a single output. However, for (thermo-)acoustic elements, pressure or velocity fluctuations on one side will in general respond to fluctuations of both pressure and velocity on the other side. Fortunately, it is possible to expand the formalism of the finite impulse response filter to this situation. Consider in a first step, a 2-to-1 filter with two input signals $s^{(1)}$ and $s^{(2)}$ and one output signal r. With suitably defined unit impulse response functions $\mathbf{h}^{(1)}$ and $\mathbf{h}^{(2)}$, one may again approximate the filter's response as

$$r_i \approx \sum_{k=0}^{L} h_k^{(1)} s_{i-k}^{(1)} + \sum_{k=0}^{L} h_k^{(2)} s_{i-k}^{(2)}. \tag{22}$$

Here, $\mathbf{h}^{(1)}$ is the response observed if a unit impulse is applied at time $t = 0$ to input "1" of the filter, and similarly for $\mathbf{h}^{(2)}$. The two impulse response functions can again be determined by solving the Wiener–Hopf equation (18). If there is more than one input, the approximations to the impulse response vector and the cross-correlation vector appearing

in this equation must be

$$\mathbf{h} = \begin{pmatrix} h_0^{(1)} \\ h_1^{(1)} \\ \vdots \\ h_L^{(1)} \\ h_0^{(2)} \\ h_1^{(2)} \\ \vdots \\ h_L^{(2)} \end{pmatrix} \quad \text{and} \quad \mathbf{c} = \frac{1}{N-L+1} \sum_{l=L}^{N} \begin{pmatrix} s_l^{(1)} r_l \\ s_{l-1}^{(1)} r_l \\ \vdots \\ s_{l-L}^{(1)} r_l \\ s_l^{(2)} r_l \\ s_{l-1}^{(2)} r_l \\ \vdots \\ s_{l-L}^{(2)} r_l \end{pmatrix}. \tag{23}$$

Similarly, the approximation of the autocorrelation matrix is now of dimension $4(L+1)^2$ with the entries

$$\Gamma = \frac{1}{N-L+1} \sum_{l=L}^{N} \begin{pmatrix} s_l^{(1)} s_l^{(1)} & \cdots & s_l^{(1)} s_{l-L}^{(1)} & s_l^{(1)} s_l^{(2)} & \cdots & s_l^{(1)} s_{l-L}^{(2)} \\ \vdots & & \vdots & \vdots & & \vdots \\ s_{l-L}^{(1)} s_l^{(1)} & \cdots & s_{l-L}^{(1)} s_{l-L}^{(1)} & s_{l-L}^{(1)} s_l^{(2)} & \cdots & s_{l-L}^{(1)} s_{l-L}^{(2)} \\ s_l^{(2)} s_l^{(1)} & \cdots & s_l^{(2)} s_{l-L}^{(1)} & s_l^{(2)} s_l^{(2)} & \cdots & s_l^{(2)} s_{l-L}^{(2)} \\ \vdots & & \vdots & \vdots & & \vdots \\ s_{l-L}^{(2)} s_l^{(1)} & \cdots & s_{l-L}^{(2)} s_{l-L}^{(1)} & s_{l-L}^{(2)} s_l^{(2)} & \cdots & s_{l-L}^{(2)} s_{l-L}^{(2)} \end{pmatrix}. \tag{24}$$

Estimating this autocorrelation matrix from time series data $s_i^{(1)}$ and $s_i^{(2)}$ obviously requires a bit more care in bookkeeping the indices, but is not fundamentally more complicated than for a one-port. Once the two impulse response functions are determined, the z-transform, applied to each of them in turn produces two transfer functions, such that in frequency space

$$\hat{r}(\omega) = F^{(1)}(\omega)\hat{s}^{(1)}(\omega) + F^{(2)}(\omega)\hat{s}^{(2)}(\omega). \tag{25}$$

If there is a filter with a second output, i.e., responses $r^{(1)}$ and $r^{(2)}$, the analysis for the 2-to-1 filter just described simply has to be carried out also for the second output (upon assuming as usual that both outputs are determined completely and solely by the two input signals). For an acoustic system with two inputs p'_u, v'_u and two outputs p'_d, v'_d, the transfer matrix $\mathbf{T}$ can be determined as

$$\mathbf{T}(\omega) = \begin{pmatrix} \check{h}^{(pp)}(\mathrm{e}^{\mathrm{i}\omega\Delta t}) & \check{h}^{(pv)}(\mathrm{e}^{\mathrm{i}\omega\Delta t}) \\ \check{h}^{(vp)}(\mathrm{e}^{\mathrm{i}\omega\Delta t}) & \check{h}^{(vv)}(\mathrm{e}^{\mathrm{i}\omega\Delta t}) \end{pmatrix}. \tag{26}$$

The four impulse response functions $h^{(pp)}$, $h^{(pu)}$, $h^{(up)}$ and $h^{(uu)}$ are determined by solving the Wiener–Hopf equation—with the generalized cross-correlation vector, equation (23), and autocorrelation matrix (24)—once for the first output p_d and then for the second output v_d.

The signal shape is quite arbitrary. Step functions, which are not easily represented accurately in a time-dependent fluid dynamics computation, can be avoided. It is merely required that the signal be persistently exciting [41]: i.e., that it has appropriate frequency content. Otherwise, Γ is ill-conditioned and the estimates for auto- and cross-correlations are not sufficiently accurate.

In principle, an $m \times n$ transfer matrix describing a multi-port or $m + n$-pole can be obtained if the signal vector $\mathbf{s}$ is defined as a suitable combination of n signals and m impulse response functions $\mathbf{h}^{(m)}$—one for each output variable of the multi-pole—are introduced.

The results presented in this section are summarized as follows. A novel method has been described, which allows one to determine the transfer matrix of an acoustic element (a "multi-port" with one or more inputs and one or more outputs) by time-dependent numerical simulation. The procedure comprises the following steps.

(1) Obtain a steady state solution for incompressible flow through the element.

(2) Generate time series of pressure and velocity (and other possible variables) up- and downstream of the element by carrying out a time-dependent computation of compressible flow with unsteady boundary conditions. The time scale of changes to the boundary conditions must be adjusted to provide adequate frequency content for the time series s_i and r_i. Also, the fluctuations of the different input quantities must be linearly independent from each other.

(3) From the time series data, compute the estimates of the auto-correlation Γ and cross-correlations $\mathbf{c}$ with equations (23) and (24). For each output, a different cross-correlation between signals and response must be computed.

(4) Solve the Wiener–Hopf equations (18) for the impulse responses $\mathbf{h}$. There is one impulse response for each combination of input and output!

(5) z-transform (see equation (21)) the impulse responses to frequency space to obtain the coefficients of the transfer matrix.

Since it is not assumed that the incoming perturbation is of a certain functional form, it is acceptable that reflections from the boundaries reach the two-port during the simulation. Indeed, the superposition of reflections with perturbations from the boundaries should help to ensure that the two-port's input signals are independent from each other.

6. τ–ζ TRANSFER MATRIX FROM INSTATIONARY CFD

As stated in the Introduction, one advantage of the proposed approach of determining the transfer matrix of an acoustic multi-port from instationary CFD is that it allows one to simulate only the element of interest and its immediate vicinity rather than the full thermoacoustic system complete with physically correct boundary conditions. In keeping with this philosophy, the domain used for the computations below is only 0·3 m long and is resolved with 100 computational cells. The heat source is located 0·02 m downstream of the inlet. Recall that the "original" τ–ζ tube is 1 m long, with the heat source in the middle; for the computational model discussed in section 3, 200 cells were used.

Mean flow conditions and model parameters were chosen to yield a transfer matrix with non-zero off-diagonal terms, i.e., inflow velocity $v_0 = 34$ m/s at a temperature $T_c = 288$ K, corresponding to a Mach number $M_c = 0{\cdot}1$ on the cold side of the heat source. The pressure loss coefficient was set to $\zeta = 5$, the power of the heat source was adjusted to have a temperature $T_h = 430$ K downstream of the heat source, resulting in an interaction index $n = 0{\cdot}25$. For the time lag, the value $\tau = 3$ ms was chosen. As for the unit step response computations, first an incompressible steady state solution was computed, where the density ρ was computed from the gas law by using the operating pressure $p_0 = 1$ bar, rather than the local static pressure. Then an unsteady run was started, with the value of the upstream inflow velocity following the profile shown in Figure 7. It is expected that the amplitude, shape and frequency content of the perturbation signal does have an impact on the quality of the estimates for the auto- and cross-correlations. Similarly, it may play a role

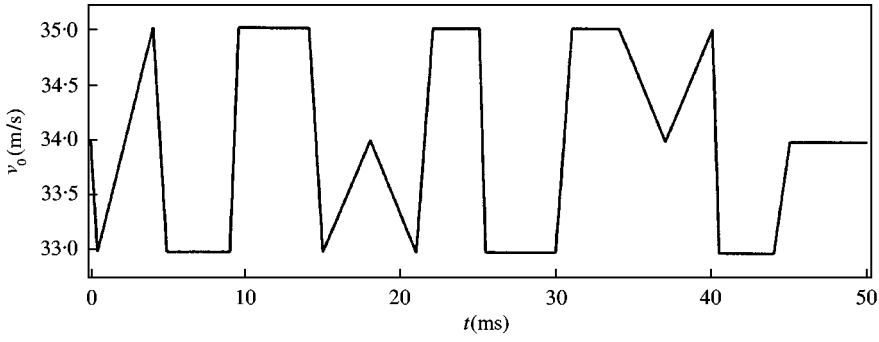

Figure 7. Unsteady inflow velocity boundary condition.

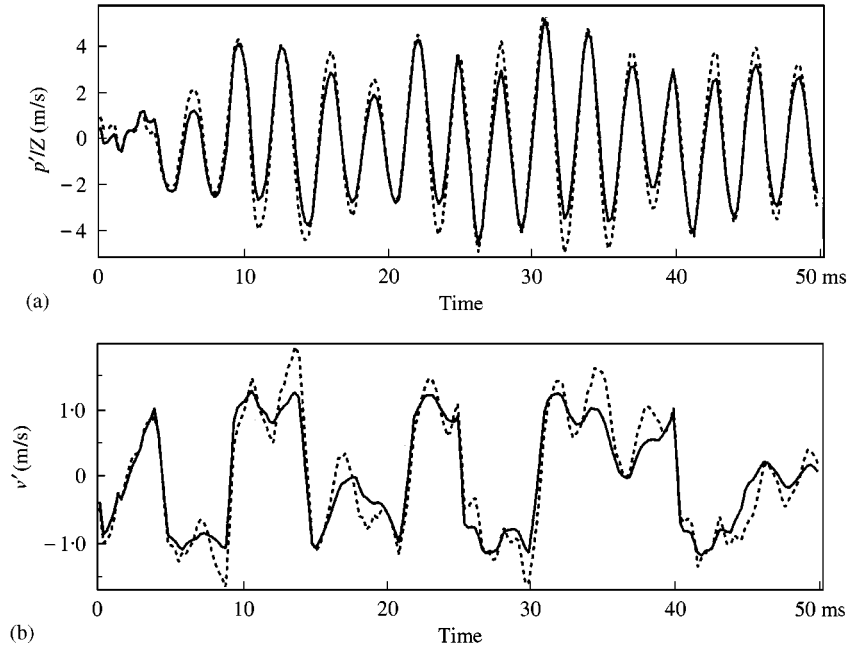

Figure 8. Pressure and velocities up- and downstream of the heat source for unsteady simulation with perturbed upstream velocity boundary condition. (a) ——, p'_c; - - -, p'_h, (b) ——, v'_c; - - -, v'_h.

whether velocity, static pressure or total pressure are perturbed. A systematic investigation of these questions will be the subject of future studies. The time step chosen was $dt = 10^{-5}$ s; however, only every 25th time step was used in the following analysis, so the effective sampling interval $\Delta t = 0{\cdot}25$ ms. The unsteady run was continued up to time $t_{max} = 50$ ms.

The time series of signals and responses, i.e., the fluctuations of pressure and velocity up- and downstream of the heat source are shown in Figure 8. Surprisingly, the pressure traces show strong oscillations with a period of approximately 3 ms, which obviously do not correlate with the velocity perturbation imposed. However, elementary analysis shows quickly that the period of 3 ms corresponds nicely to the quarter-wave eigenmode of the present computation model with a tube length $L = 0{\cdot}3$ m. The obvious conclusion is that although the chosen time lag $\tau = 3$ ms results in very strong decay of perturbations for the

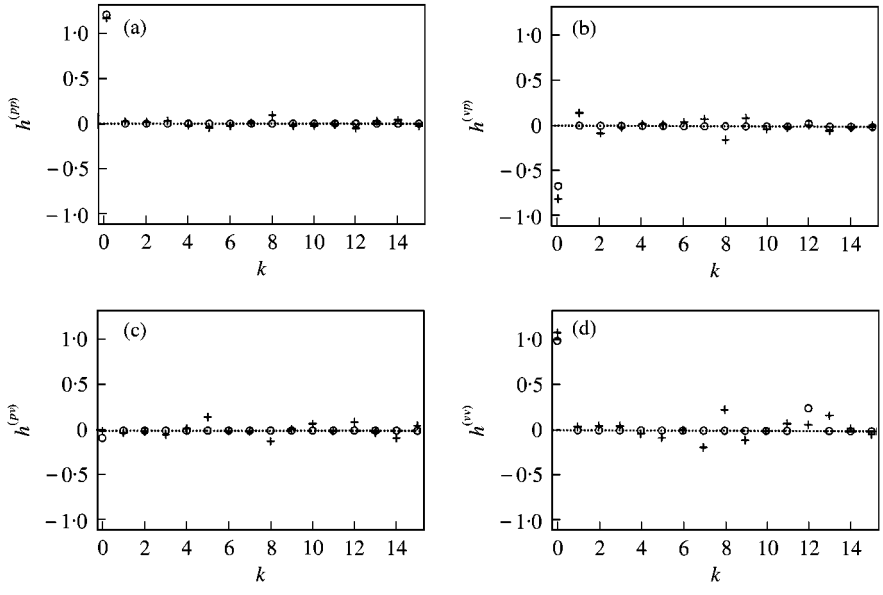

Figure 9. Unit impulse responses of the τ–ζ model obtained from unsteady simulation with perturbed inflow velocity boundary condition. Upper left: $\mathbf{h}^{(pp)}$, upper right: $\mathbf{h}^{(vp)}$, lower left: $\mathbf{h}^{(pv)}$, lower right: $h^{(vv)}$. Computational (+) and theoretical results (○) for the h_k's, $k = 0, \ldots, 15$ are shown. Note the different vertical axis scalings.

"original" τ–ζ tube with length 1 m, it produces a (weak) thermoacoustic instability for the system with length 0·3 m. The velocity signals in Figure 8 show the influence of the oscillations with a period of 3 ms superposed on the fluctuations due to the unsteady upstream boundary condition. Comparing the velocity profiles at the inlet (Figure 7) and at the cold side of the heat source (v'_h in Figure 8), shows that very little smearing out due to numerical dissipation is found. The signal gradients appear steep enough to provide sufficient high-frequency content. Differences between the velocity profiles v'_0 and v'_c are mainly due to the influence of the pressure oscillations. In any case, these differences are not a source of error for the present method, because no particular shape of the perturbation signal is required. Whatever pressure and velocity fluctuations are observed at the inputs of the multi-port are accepted as the signal for the estimation of the auto- and cross-correlation. This is an essential difference between the present method and the unit step approach [22, 26], where it is required that a step perturbation is given as the signal to the multi-port.

The impulse responses derived from the pressure and velocity time series are shown in Figure 9. Here the length of the impulse response vector was set to $L = 16$. With the chosen time lag $\tau = 3$ ms $= 12\Delta t$, the delayed part of the response should appear in h_{12}. Except for the first coefficient h_0, which describes the immediate response to a signal, the computed unit impulse response vectors show quite strong deviations from the expected values, especially for $\mathbf{h}^{(pv)}$. However, the unit impulse responses are not of interest *per se*, as it is the transfer matrix, derived from the unit responses by the z-transformation, which is used in network analysis. Fortunately, here the agreement between the theoretical and numerical results is much better; see Figure 10. With the exception of the absolute value of the velocity–velocity coupling $T^{(vv)}$ (lower right coefficient) and the phase of the pressure–velocity coupling $T^{(pv)}$ (lower left coefficient), the agreement is not only qualitatively but also quantitatively very satisfactory. This is in particular so in the

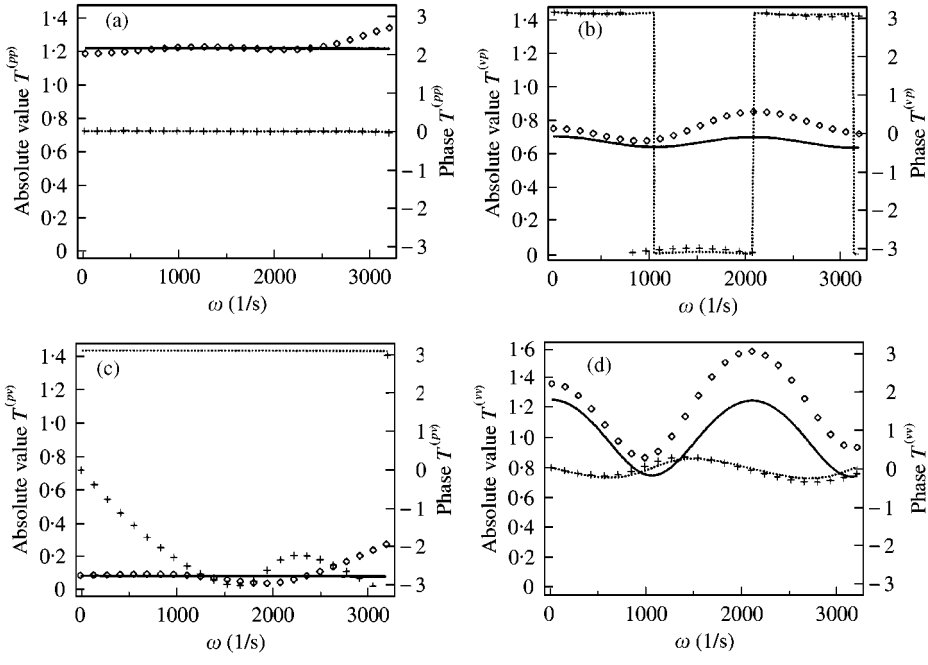

Figure 10. Coefficients of the transfer matrix $\mathbf{T}(\omega)$ of the τ–ζ model obtained from unsteady simulation with a perturbed velocity boundary condition. Upper left: $T^{(pp)}$, Upper right: $T^{(vp)}$, lower left: $T^{(pv)}$, lower right: $T^{(vv)}$. Computational ($\diamond$) and theoretical results (—) for the absolute value (left axis) as well as Computational (+) and theoretical results (– – –) for the phase (right axis) are shown.

frequency range $\omega \approx 600$–$700\ \mathrm{s}^{-1}$, where the first eigenmode of the τ–ζ tube is found (cf. Figure 3).

This analysis was repeated with data from a second unsteady simulation with different boundary conditions, i.e. prescribed total pressure upstream and static pressure downstream. During the unsteady run both pressure boundary conditions were varied in a way similar to the velocity boundary condition used in the first case; see Figure 7. The rationale for this modification was that the influence of the periodic pressure oscillations on the accuracy of the results achieved was not known. By changing the boundary type and varying both boundary conditions in time, it was hoped that the unstable acoustic mode would not develop during the run. This expectation was fulfilled; the pressure and velocity signals produced by the second unsteady simulation appear to be mainly the response to the perturbations imposed at the boundaries; see Figure 11. However, it is observed that these modifications did not improve the prediction of the unit impulse response or the transfer matrix; see Figures 12 and 13. As a matter of fact, for the pressure–velocity coupling, the agreement between theory and simulation is worse than it was for the previous run.

Nevertheless, the results achieved with the novel method are satisfactory. Indeed, when comparing with the level of quality and consistency that can be achieved with experimental methods [17–19] to determine transfer matrices—and considering the effort that is required to obtain such results—the performance of the CFD-based approach presented in this paper is rather impressive. All four coefficients of the transfer matrix are obtained with acceptable accuracy in magnitude and phase for frequencies below $1000\ \mathrm{s}^{-1}$, where the first eigenmode of the system is found. At higher frequencies, the deviations increase in magnitude, but this frequency range is of minor importance for the present model. The

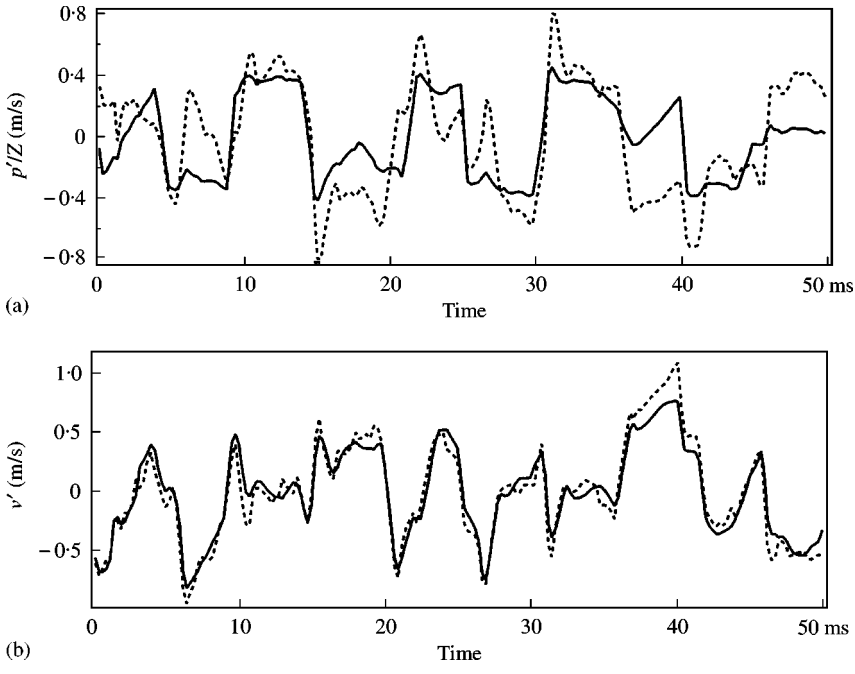

Figure 11. Fluctuations of pressure (top) and velocity (bottom) observed for the case with time-varying total pressure (inflow) and static pressure (outflow) boundary conditions. (a) ——, p'_c; - - -, p'_h, (b) ——, v'_c; - - -, v'_h.

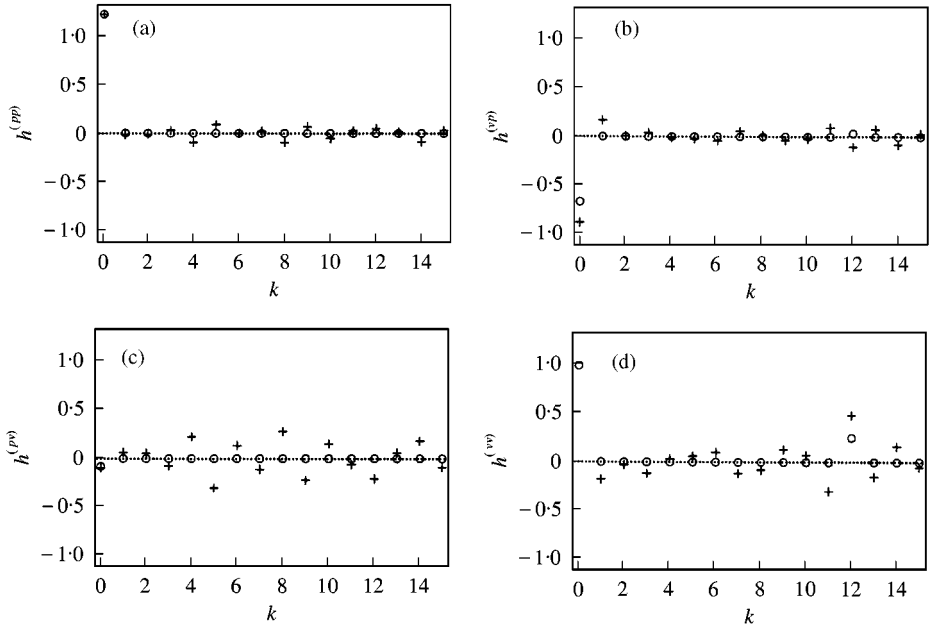

Figure 12. Unit impulse responses of the τ–ζ model obtained from unsteady simulation with perturbed pressure boundary conditions. Upper left: $\mathbf{h}^{(pp)}$, upper right: $\mathbf{h}^{(vp)}$, lower left: $\mathbf{h}^{(vp)}$, lower right: $\mathbf{h}^{(vv)}$. Computational (+) and theoretical results (○) for the h_k's, $k = 0, \ldots, 15$ are shown. Note the different vertical axis scalings.

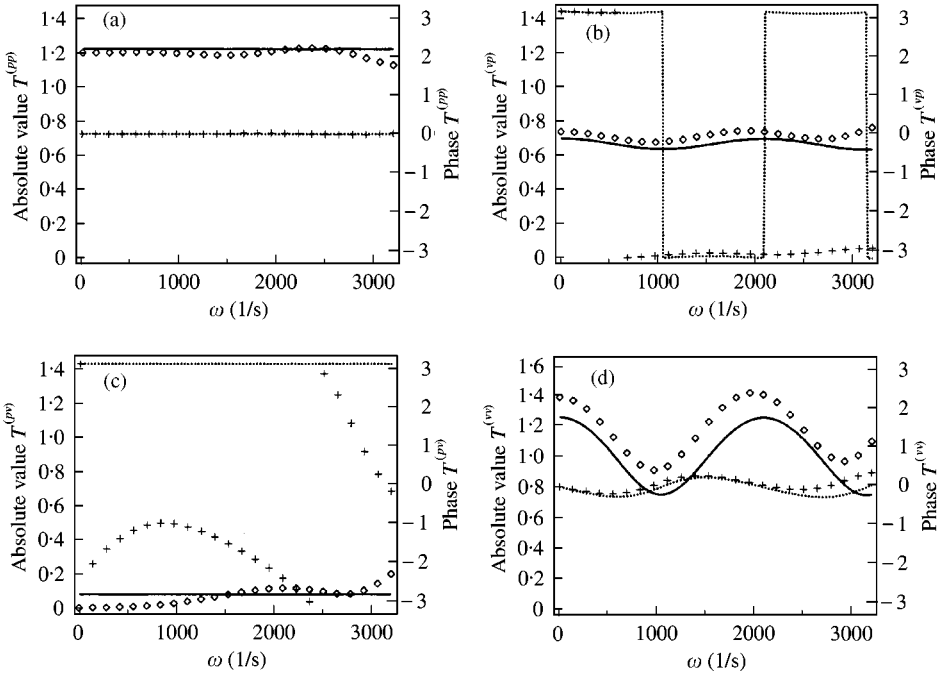

Figure 13. Coefficients of the transfer matrix $\mathbf{T}(\omega)$ of the τ–ζ model obtained from unsteady simulation with perturbed pressure boundary conditions. Upper left: $T^{(pp)}$, Upper right: $T^{(vp)}$, lower left: $T^{(vp)}$, lower right: $T^{(vv)}$. Computational ($\diamond$) and theoretical results (—) for the absolute value (left axis) as well as Computational (+) and theoretical results (– – –) for the phase (right axis) are shown.

algorithm is obviously able to disentangle the interactions of pressure and velocity perturbations propagating in the upstream and downstream direction across the heat source. The total amount of data used—length $N = 200$ of the time series, equivalent to 50 ms—for the analysis is quite small. Indeed, the 50 ms compare very favorably with the direct CFD analysis presented in section 3, were even for a very strongly unstable or stable case, the unsteady simulation has to evolve for several hundred ms before the long-time state (limit cycle or steady flow) is approached. For a system near the stability limit, computation times would be much longer.

7. SUMMARY AND CONCLUSIONS

An efficient and often adequate description of the (thermo-) acoustic properties of a combustion system is offered by acoustic filter or multi-port networks. The representation of a combustion system with these tools requires knowledge of the transfer matrices of the system's constitutive multi-ports. For simple multi-ports, the transfer matrix can be derived from the (linearized) equations of conservation of mass and momentum and suitable additional assumptions. However, in general, the determination of the transfer matrix from first principles is intractable and one has to resort to experimental or numerical simulation.

It has been suggested previously to determine the acoustic properties of an acoustic element from time-dependent numerical simulation of the response of the element to a sudden disturbance. Specifically, the response—in terms of the mass flux across the flame—to a unit-step perturbation is Laplace-transformed to obtain the (scalar) frequency

response function. The present work extends these ideas by employing more advanced tools from communications engineering: i.e., system identification. Specifically, the multi-port is regarded as a finite impulse response filter, and its unit impulse responses are determined by solving the Wiener–Hopf equation. The required auto- and cross-correlations of signal and filter response are estimated from time series data obtained from a time-dependent simulation of the multi-port's response to a perturbation of upstream or downstream boundary conditions. Finally, the transfer matrix required for network analysis is obtained by a z-transform of the impulse responses.

It is noteworthy that this novel approach is not limited to a scalar frequency response function. The 2×2 transfer matrix describing a two-port filter can be obtained from one single time-dependent computation. Extensions of the method to matrices of higher dimension seem feasible for multi-ports with more than two ports and/or additional variables representing, e.g., fluctuating fuel concentration or entropy. Furthermore, the use of step functions, which are required for the unit step approach with subsequent Laplace-transform, but which are not easily represented accurately in a time-dependent fluid dynamics computation, can be avoided. Indeed, the shape of the perturbation signal is quite arbitrary, it is merely necessary that the signal possesses sufficient frequency content and is persistently exciting. For the same reason, it is also permissible that reflections of the original perturbation from the boundaries of the computational domain impinge upon the two-port. The instationary simulation may therefore be continued beyond the time which an acoustic perturbation requires to travel back and forth across the computational domain. Longer simulation times are expected to lead to more accurate estimates of cross- and auto-correlations of signal and response. Finally, there is no minimum frequency spacing for the transfer matrix, as exists for the inverse Laplace transformation method.

The method has been successfully applied to a one-dimensional model of a heat source with time delay placed in a low-Mach-number compressible flow, for which an analytical description can be derived from first principles. Computational predictions of the transfer matrix have been validated successfully against these analytical results.

Applications of the method to two-dimensional purely acoustic (i.e., without heat release) two-ports shall be reported elsewhere; applications to turbulent reacting flows in premix burners are planned.

ACKNOWLEDGMENTS

We gratefully acknowledge the contributions of Hans Gijrath and Johan Löfgren to this study, who showed much enthusiasm, diligence and perseverance during their diploma works.

REFERENCES

1. R. L. RAUN, M. W. BECKSTEAD, J. C. FINLINSON and K. P. BROOKS 1993 *Progress in Energy and Combustion Science* **19**, 313–364. A review of Rijke tubes. Rijke burners and related devices.
2. J. W. S. RAYLEIGH 1896 *The Theory of Sound*. London: Macmillan.
3. W. POLIFKE, C. O. PASCHEREIT and T. SATTELMAYER 1997 A universally applicable stability criterion for complex thermoacoustic systems. 18. *Deutsch-Niederländischer Flammentag*, vol. 1313, 455–460, Delft, NL: VDI Bericht, 1997.
4. T. SATTELMAYER and W. POLIFKE 2001 A novel method for the computation of thermo-acoustic stability: submitted to *Comb. Sci. Tech.*, 2001.
5. D. VEYNANTE and T. POINSOT 1997 *Annual Research Briefs*, Center for Turbulence Research, 253–274. Large Eddy simulation of combustion instabilities in turbulent premixed burners.

6. R. LIU 1998 *Seventh International Conference on Numerical Combustion, York, UK*. Modelling of the combustion oscillations of a turbulent premixed flame.
7. C. HANTSCHK and D. VORTMEYER 1999 *Journal of Sound and Vibration*, **3**, 511–522. Numerical Simulation of Self-Excited Thermoacoustic Instabilities in a Rijke Tube.
8. T. MUROTA and M. OHTSUKA 1999 *International Gas Turbine and Aeroengine Congress & Exposition*, ASME Paper 99-GT-274. New York: ASME. Large-Eddy simulation of combustion oscillation in premixed combustor.
9. R. C. STEELE, L. H. COWELL, S. M. CANNON and C. E. SMITH 1999 *International Gas Turbine and Aeroengine Congress & Exposition*, ASME Paper 99-GT-052. Passive control of combustion instability in lean premixed combustors.
10. S. J. BROOKES, R. S. CANT, D. J. DUPERE and A. P. DOWLING 2000 *International Gas Turbine and Aeroengine Congress & Exposition*, Munich, Germany. ASME Paper 2000-GT-104. Computational modelling of self-excited combustion instabilities.
11. H. G. SUNG, S. Y. HSIEH and V. YANG 2000 28*th Symposium* (*International*) *on Combustion, Edinburgh, Scottland*. Combustion dynamics of a lean-premixed swirl-stabilized injector.
12. M. L. MUNJAL 1986 *Acoustics of Ducts and Mufflers*. New York: John Wiley & Sons.
13. J. J. KELLER 1995 *American Institute of Aeronatics and Astronautics Journal* **33**, 2280–2287. Thermoacoustic oscillations in combustion chambers of gas turbines.
14. G. C. HSIAO, R. P. PANDALAI, H. S. HURA and H. C. MONGIA 1998 34*th Joint Propulsion Conference & Exhibit*, AIAA 98-3380. New York: AIAA, ASME, SAE, ASEE, July. Combustion dynamic modeling for gas turbine engines.
15. G. C. HSIAO, R. P. PANDALAI, H. S. HURA and H. C. MONGIA 1998 34*th Joint Propulsion Conference & Exhibit*, AIAA 98–3381, July. Investigation of combustion dynamics of dry-low-emission (DLE) gas turbine engines.
16. W. POLIFKE, C. O. PASCHEREIT and K. DÖBBELING 1999 *Sixth International Conference on Sound and Vibration, Copenhagen, Denmark*. Suppression of combustion instabilities through destructive interference of acoustic and entropy waves.
17. C. O. PASCHEREIT and W. POLIFKE 1998 *International Gas Turbine and Aeroengine Congress & Exposition, Stockholm*. ASME Paper 98-GT-582. Investigation of the thermo-acoustic characteristics of a lean premixed gas turbine burner.
18. B. B. H. SCHUERMANS, W. POLIFKE and C. O. PASCHEREIT 1999 *International Gas Turbine and Aeroengine Congress & Exposition*, ASME Paper 99-GT-132. Indianapolis, Indiana, USA. Modeling transfer matrices of premixed flames and comparison with experimental result.
19. B. B. H. SCHUERMANS, W. POLIFKE and C. O. PASCHEREIT 2000 *International Gas Turbine and Aeroengine Congress & Exposition, Munich, Germany*. ASME Paper 2000-GT-105. Prediction of acoustic pressure spectra in gas turbines based on measured transfer matrices.
20. A. P. DOWLING 1999 *Sixth International Congress on Sound and Vibration, Copenhagen, Denmark*, 3277–3292. Thermoacoustics instability.
21. T. SATTELMAYER 2000 *International Gas Turbine and Aeroengine Congress & Exposition, Munich, Germany*. ASME Paper 2000-GT-82. Influence of the combustor aerodynamics on combustion instabilities from equivalence ratio fluctuations.
22. E. DEUKER 1995 *Ph.D. Thesis, RWTH Aachen*. Ein Beitrag zur Vorausberechnung des akustichen Stabilitätsverhaltens von Gasturbinen-Brennkammern mittels theoretischer und experimenteller Analyse von Brennkammerschwingungen.
23. L. CREMER 1971 *Journal of Sound and Vibration* **16**, 1–15. The second annual fairy lecture: the treatment of fans as black boxes.
24. H. BODÉN and M. ÅBOM 1995 *Acta Acustica* **3**, 549–560. Modelling of fluid machines as sources of sound in duct and pipe systems.
25. J. LAVRENTJEV and M. ÅBOM 1996 *Journal of Sound and Vibration* **197**, 1–16. Characterization of fluid machines as acoustic multi-port sources.
26. V. A. SKLYAROV and V. I. FURLETOV 1975 *Zhurnal Prikladnoi Mekhaniki i Tekhnicheskoi Fiziki*, **1, UDC 536.46:533.6**, 84–94. Frequency characteristics of a laminar flame.
27. D. BOHN and E. DEUKER 1993 *20th International Congress on Combustion Engines*, Paper G20 CIMAC, London, UK. An acoustical model to predict combustion driven oscillations.
28. U. KRÜGER, S. HOFFMANN, W. KREBS, H. JUDITH, D. BOHN and G. MATOUSCHEK 1998 *International Gas Turbine and Aeroengine Congress & Exposition, Stockholm, Sweden*. ASME Paper 98-GT-323. Influence of turbulence on the dynamic behaviour of premixed flames.

29. U. KRÜGER, J. HÜREN, S. HOFFMANN, W. KREBS and D. BOHN 1999 *International Gas Turbine and Aeroengine Congress & Exposition, Indianapolis, IN*. ASME Paper bf 99-GT-111. Prediction of thermoacoustic instabilities with focus on the dynamic flame behavior for the 3A-series gas turbine of Siemens KWU.
30. M. HECKL 1988 *Journal of Sound and Vibration* **124**, 117–133. Active control of the noise from a "Rijke" tube.
31. K. R. MCMANUS, T. POINSOT and S. M. CANDEL 1993 *Progress Energy Combustion Sciences* **19**, 1–29. A review of active control of combustion instabilities.
32. B. T. CHU 1953 *Fourth Symposium* (*International*) *on Combustion*, 603–612. On the generation of pressure waves at a plane flame front.
33. W. POLIFKE, A. FISCHER and T. SATTELMAYER 2001 *International Gas Turbine and Aeroengine Congress & Exposition*, New York: New Orleans, LO. ASME. Instability of premix burner with non-monotonic pressure drop characteristic.
34. H. GIJRATH 1997 *Master's Thesis, ABB Corporate Research and Delft University of Technology*. An analytical and numerical investigation of thermo-acoustic instability problems.
35. J. LÖFGREN 1998 *Master's Thesis ABB Corporate Research and University of Uppsala*. Determination of acoustic transfer matrices by time-dependent numerical simulation.
36. E. TURKEL, V. N. VATSA and R. RADESPIEL 1996 Technical Report 96-57, October. Preconditioning methods for low-speed flows.
37. T. KAILATH 1980 *Linear Systems*. Englewood Cliffs, NJ: Prentice-Hall.
38. H. UNBEHAUEN 1963 *Regelungstechnik* **12**, 551–555. Ein graphisch-analytisches Rechenverfahren zur Bestimmung des Frequenzganges aus der Übergangsfunktion.
39. M. BELLANGER 1984 *Digital Processing of Signals*. New York: Wiley Interscience.
40. T. SÖDERSTRÖM and P. STOICA 1989 *System Identification*. Englewood Cliffs, NJ: Prentice-Hall.
41. L. LJUNG 1999 *System Identification—Theory For the User*. Englewood Cliffs, NJ: Prentice-Hall: Second edition.

APPENDIX A

In this section it is illustrated—by using the n–τ model as an example—how the frequency response of a linear system may be recovered as the Laplace transform of its unit step response. A general proof of these statements is given, e.g., by Kailath [37].

Consider a linear system with a real-valued input signal s and a real-valued output signal or response r. Then the frequency response function $F(\omega)$, which satisfies

$$\hat{r}(\omega) = F(\omega)\hat{s}(\omega)$$

for the Fourier transforms $\hat{r}$ and $\hat{s}$ of signal and response, is equal to

$$F(\omega) = \left.\frac{\mathscr{L}_r(z)}{\mathscr{L}_s(z)}\right|_{z=\mathrm{i}\omega}. \tag{A1}$$

On the r.h.s., $\mathscr{L}_f(z) \equiv \int_0^\infty f(t)\,\mathrm{e}^{-zt}\,\mathrm{d}t$ denotes the one-sided Laplace transform of some function f. Now consider the special case of the response $u(t)$ of the system to a unit step or Heaviside signal

$$s(t) = H(t) \equiv \begin{cases} 0 & \text{for } t < 0, \\ 1 & \text{for } t \geqslant 0. \end{cases}$$

It follows with $\mathscr{L}_H(z) = 1/z$ from equation (A1) that

$$F(\omega) = z\mathscr{L}_u|_{z=\mathrm{i}\omega} = \mathrm{i}\omega \int_0^\infty u(t)\,\mathrm{e}^{-\mathrm{i}\omega t}\,\mathrm{d}t. \tag{A2}$$

For the n–τ model, the response $u(t)$ to a unit step perturbation is shown in Figure 5. Obviously,

$$\mathscr{L}_u = \int_0^\infty \mathrm{e}^{-zt}\,\mathrm{d}t + (1+n)\int_\tau^\infty \mathrm{e}^{-zt}\,\mathrm{d}t = \frac{1}{z}(1 + n\,\mathrm{e}^{-z\tau}),$$

and one reproduces the frequency transfer function $F(\omega) = 1 + n\exp(-\mathrm{i}\omega\tau)$ of the n–τ model.

APPENDIX B

In this section, it is demonstrated that the z-transform $\check{h}(z)$ of the unit impulse response $\mathbf{h}$ with argument $z = \exp\{\mathrm{i}\omega\Delta t\}$ indeed yields the frequency response function of a linear filter.

First, recall that the discrete forward Fourier transform of $N+1$ sample points $s_k \equiv s(t_k)$ with sampling interval Δt and $t_k = k\Delta t$, $k = 0, 1, 2, \ldots, N$, is defined as

$$\hat{s}(\omega_k) \equiv \hat{s}_k \equiv \sum_{n=0}^{N} \exp\left\{-\mathrm{i}\frac{2\pi n k}{N+1}\right\} s_n, \tag{B1}$$

where $\hat{s}$ is the discrete Fourier transform, and the sample points in frequency space are $\omega_k = 2\pi k/(N+1)\Delta t$.

Now consider the discrete Fourier transform of the response r of a linear filter,

$$\hat{r}_k = \sum_{n=0}^{N} \exp\left\{-\mathrm{i}\frac{2\pi n k}{N+1}\right\} r_n \tag{B2}$$

$$= \sum_{n=0}^{N} \exp\left\{-\mathrm{i}\frac{2\pi n k}{N+1}\right\} \sum_{j=0}^{L} h_j s_{n-j}. \tag{B3}$$

Substituting for s_{n-j} with the definition of the inverse discrete Fourier transform

$$s_k = \frac{1}{N+1}\sum_{n=0}^{N} \exp\left\{-\mathrm{i}\frac{2\pi n k}{N+1}\right\} \hat{s}_n, \tag{B4}$$

and then using the series representation of the Kronecker δ,

$$\delta_{k,m} = \frac{1}{N+1}\sum_{n=0}^{N} \exp\left\{-\mathrm{i}\frac{2\pi(k-m)n}{N+1}\right\}, \tag{B5}$$

to eliminate double summations, one can simplify equation (B3) to obtain

$$\hat{r}_k = \sum_{j=0}^{L} h_j \exp\left\{-\mathrm{i}\frac{2\pi k j}{N+1}\right\} \hat{s}_k. \tag{B6}$$

With $2\pi k/(N+1) = \omega_k\Delta t$ and the definition of the z-transform $\check{h}(z) = \sum_{j=0}^{L} h_j z^{-j}$ this yields

$$\hat{r}_k = \check{h}(\mathrm{e}^{\mathrm{i}\omega_k\Delta t})\hat{s}_k. \tag{B7}$$

APPENDIX C: NOMENCLATURE

Upper case letters

A	cross-sectional area
F	scalar frequency response function
$\mathrm{Im}(z)$	imaginary part of complex variable z
$\mathrm{Re}(z)$	real part of complex variable z
H	Heaviside step function (unit step)
L, M, N	integers
$\mathscr{L}_f$	Laplace transform of function f
$\dot{Q}$	rate of heat release per unit area
M	Mach number
$\mathbf{S}$	system matrix
T	temperature
$\mathbf{T}$	transfer matrix
$T^{(vv)}$	coefficient of transfer matrix
Z	specific impedance

Lower case letters

c	speed of sound
$\mathbf{c}$	approximation of the cross-correlation of signal and response
$\mathbf{h}$	impulse response vector
h_k	element of impulse response
p	pressure
$\mathbf{r}, r_i$	response
$\mathbf{s}$	signal
u	step response
$\mathbf{u}$	vector of unknowns
v	velocity
x	spatial co-ordinate
z	complex variable

Greek letters

α	area ratio, A_u/A_d
γ	ratio of specific heats
Γ	approximation of the autocorrelation matrix of a signal
δ	cycle increment
δ_{ik}	Kronecker delta
λ	reduced length
ω	angular frequency
ρ	density
τ	time lag
ξ	ratio of specific impedances up- and downstream
ζ	pressure loss coefficient

Subscripts and accents

0	inlet
c	cold
h	hot
x	exit
d	downstream
u	upstream
$\hat{f}$	Fourier transform of function f
$\tilde{h}(z)$	z-transform of unit impulse response vector $\mathbf{h}$
$\check{h}(z)$	expectation value
$\tilde{r}$	expectation value of r